mathematics

MDPI

Article

Sensitive Channel Selection for Mental Workload Classification

Lin Jin [1], Hongquan Qu [1], Liping Pang [2,*] and Zheng Zhang [1]

[1] School of Information Science and Technology, North China University of Technology, Beijing 100144, China; jinlin@mail.ncut.edu.cn (L.J.); qhqphd@ncut.edu.cn (H.Q.); zhangzheng@ncut.edu.cn (Z.Z.)
[2] School of Aeronautic Science and Engineering, Beihang University, Beijing 100191, China
* Correspondence: pangliping@buaa.edu.cn

Abstract: Mental workload (MW) assessment has been widely studied in various human–machine interaction tasks. The existing researches on MW classification mostly use non-invasive electroencephalography (EEG) caps to collect EEG signals and identify MW levels. However, the activation region of the brain stimulated by MW tasks is not the same for every subject. It may be inappropriate to use EEG signals from all electrode channels to identify MW. In this paper, an EEG rhythm energy heatmap is first established to visually show the change trends in the energy of four EEG rhythms with time, EEG channels and MW levels. It can be concluded from the presented heatmaps that this change trend varies with subjects, rhythms and channels. Based on the analysis, a double threshold method is proposed to select sensitive channels for MW assessment. The EEG signals of personalized selected channels, named positive sensitive channels (PSCs) and negative sensitive channels (NSCs), are used for MW classification using the Support Vector Machine (SVM) algorithm. The results show that the selection of personalized sensitive channels generally contributes to improving the performance of MW classification.

Keywords: mental workload classification; EEG; heatmap; sensitive channels

MSC: 68T01

Citation: Jin, L.; Qu, H.; Pang, L.; Zhang, Z. Sensitive Channel Selection for Mental Workload Classification. *Mathematics* **2022**, *10*, 2266. https://doi.org/10.3390/math10132266

Academic Editors: Jakub Nalepa and Paolo Crippa

Received: 14 May 2022
Accepted: 25 June 2022
Published: 29 June 2022

1. Introduction

In recent decades, the roles of operators tend to be as decision makers and monitors instead of manual workers in a modern human–machine system. The mental workload (MW) can be regarded as the proportion of information processing capability used to perform a task, which is determined by the amount of resources required by a set of concurrent tasks, as well as by the use of resources needed to perform them [1]. Studies have shown that an excessive MW lasting for a long time can cause rapid fatigue, frustration, reduced flexibility and increased mistakes; but too low a MW can lead to the waste of resources and dissatisfaction, which might reduce job performance [2]. Thus, the major problem in the human–machine system is being able to measure MW levels. It is important to research the control of MW, fatigue and stress levels for busy human–machine interface operators [3–5].

The original method to evaluate MW levels is achieved by filling scales. However, it is possible to use physiological signals to evaluate MW due to the particularity of operators' work in modern brain–computer interface (BCI) systems. Existing methods to evaluate MW levels use subjective measurement, performance measurement and psychophysiological measurement [6]. The first is based on the real feelings of operators measured by the National Aeronautics and Space Administration Task Load Index (NASA-TLX) scale [7]; the second is based on the operation of the main tasks by the operators; and the third is based on the physiological signals of operators including those measured by electroencephalogram (EEG), event-related brain potential (ERP), electrooculogram (EOG) and electrocardiogram (ECG), etc. [6,8]. The principle behind MW classification

by physiological signals is based on comparing significant feature differences in the time domain and frequency domain at different MW levels [9]. These features contribute to building predictable classification models. With the development of BCI technology [10–12] and machine learning, there is growing proof of the advantages of psychophysiological measurement in MW level assessment, and many studies have focused on MW prediction by using classifiers established by EEG signals [13–17].

BCI technology is classified as invasive and non-invasive. The latter is extensively used at present for safety purposes despite the former achieving a higher accuracy [18]. Based on the functions of different brain partitions, non-invasive BCI has a multi-channel nature, and some electrode placement schemes on human scalps were recommended by the International Federation [19,20]. Relevant studies show that the main useful information about MW lay in five frequency bands [21–23]. Because of the multi-channel nature of non-invasive BCI and the dividing of the frequency domain, there is an added computational complexity to the system and a reduction in the pertinence of feature extraction, which may cause dimension disaster or low classification accuracy.

Many existing MW classification methods use the EEG rhythm energies of all channels [24], and dimension reduction algorithms or transfer learning algorithms are usually necessary to solve this problem. Feature dimension reduction can also be solved by channel selection, and many efforts have been made in the selection of EEG channels. Alotaiby et al. summarized the application of EEG channel selection to classification problems in several fields [25]. The results confirmed the contribution of existing EEG channel selection strategies. Alyasser et al. promoted an EEG channel selection method based on the binary flower pollination algorithm (FPA) and β-hill climbing for personal identification [26], which showed that half of the channel numbers can achieve high accuracy. Li et al. applied the Gradient Class Activation Mapping (Grad-CAM) visualization technology on raw EEG signals to the channel selection [27]. The results achieved an optimal tradeoff between performance and the number of channels for EEG intention decoding. Moctezuma et al. applied the non-dominated sorting genetic algorithms (NSGA) to select EEG channels [28]. Park et al. compared channel selection results based on binary PSO (BPSO), BPSO with a channel impact factor, a genetic algorithm (GA) and harmony search (HS) [29]. Most of these researchers focused the channel selection on an optimization problem rather than revealing the relationship between features and EEG channels.

In existing research, many studies have shown that the regular variation between the EEG energy of the four rhythms and MW levels is not the same in different regions. Chen et al. analyzed the Power Spectral Density (PSD) of the channels Fp1, Fp2, Tp9 and Tp10 by three-way analysis of variance (ANOVA) and showed that the channel Fp1, especially the gamma band, had the highest correlation with the MW level [21]. Zhu et al. used three graph features of EEG data to analyze the relationship between different channels. The result showed that channels O2, T8, FC6, F8 and AF4 were considered optimal for a more efficient estimation of cognitive load [30]. Wang et al. used a mental workload index including the ratio of frontal theta power and parietal alpha power to analyze mental workload [23]. The result showed that the theta band activity of the frontal lobe increased significantly with the increase in task demand, while there was a decrease in alpha band activity in the parietal lobe. Altahat et al. analyzed the curve of Detection Error Tradeoff (DET) using different enhancement threshold values [31]. The result revealed that it was helpful to use combined frequency rhythms rather than a single rhythm and the personalized EEG channel set to classify the MW.

Our study firstly builds heatmaps of EEG energy to find the personalized activation regions of the brain stimulated by MW tasks for individual subjects. Then a double threshold method is proposed to select personalized sensitive channels for MW classification. The rest of this paper is organized as follows: Section 2 introduces the EEG signal acquisition experiments and data preprocessing. Subsequently, the principle of the sensitive channel selection method based on energy visualization and feature extraction is presented in detail. Section 3 applies the proposed method to classify MW levels and compares the results

with those without personalized sensitive channel selection. Lastly, Section 4 discusses the summary results and next steps.

2. Materials and Methods

This paper attempts to explore the relationship between EEG rhythm energy and the change in MW, and then conducts sensitive channel selection and feature extraction.

2.1. Experiments and Data Preprocessing

In this section, we will describe the EEG signal acquisition experiments and EEG signal preprocessing process.

2.1.1. Experiments

Two levels of MW were set on the multi-attribute task battery (MATB-II) developed by the National Aeronautics and Space Administration (NASA) [32], namely low mental workload (LMW) and high mental workload (HMW). Different MW levels during the fixed test time, 12 min, were induced by the different activation frequencies of four types of flight tasks, namely the system monitoring, tracking, scheduling and resource management tasks, respectively [33]. The four tasks correspond to numbers 1, 2, 3 and 4 in Figure 1. The details of each task are shown in Table 1. It should be noted that the time of each task and the order of multiple tasks were set as random values.

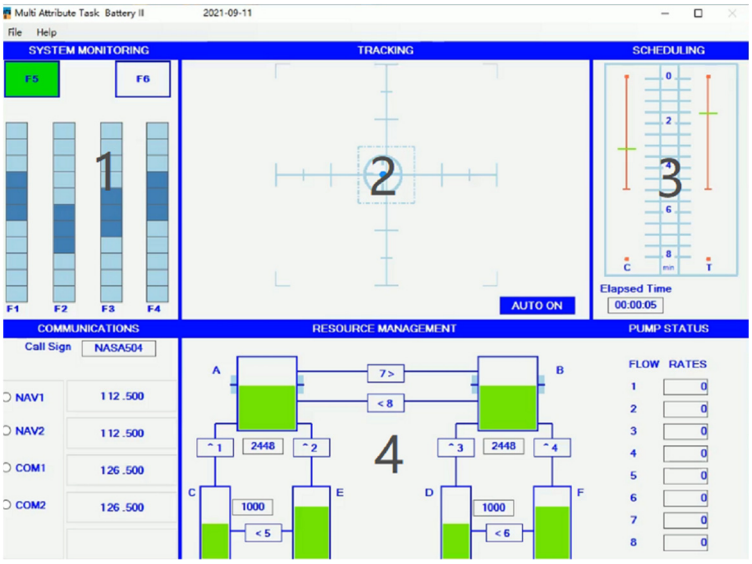

Figure 1. Area 1, 2, 3 and 4 are four tasks interface of MATB-II.

Thirty-two EEG electrode channels (Fp1, Fp2, F11, F7, F3, Fz, F4, F8, F12, FT11, FC3, FCz, FC4, FT12, T7, C3, Cz, C4, T8, CP3, CPz, CP4, M1, M2, P7, P3, Pz, P4, P8, O1, Oz and O2) were placed on the scalp of the subject mainly according to 10–20 international electrode system [19]. M1 was set as the reference while collecting EEG signals by using the Neuroscan Neuamps system (Synamps2, Scan 4.3, EI Paso, TX, USA). The recording bandwidth was 0.1–200 Hz and the digital sampling rate was 1024 Hz.

According to the selection criteria of "high performance" and "less artifacts", the EEG signals of 10 participants with engineering knowledge background in Beihang University (aged 23.4 $\pm$ 0.8 years, with 2 females and 8 males) were selected to analyze. The subject number is represented by m (m = 1, 2, . . . , 10) and it can be labeled as Sub1–Sub10. The criterion of "high performance" meant the accuracy rate of operating performance should be greater than 90% and the criterion of "less artifacts" meant the artifacts should be less than 40% of original EEG signals. All participants had trained for 15 days before the experiment to become familiar with operating instruments and different tasks in MATB-II.

In formal experiments, the one-day experiment was divided into two stages (morning and afternoon), and the experiment tasks of each stage consisted of one LMW test and one HMW test. Subjects had a 5-min rest at the beginning and end of every test. The experiment design adopted the Latin square method to eliminate the influence of LMW and HMW test sequences on EEG signals. EEG signals of every subject in LMW and HMW experiments were collected during two-day experiments. The NASA-TLX scale was also filled immediately after every MATB task to subjectively evaluate the MW state.

Table 1. Details of four tasks.

Title	Description	Activation Frequency	
		LMW	HMW
System Monitoring	Monitor the scales of F1–F4 in Area 1 and respond with a mouse when the scales are not around the center	1	24
Tracking	In Area 2, keep the target at the grid center by joystick in MANUAL mode and no action is required in AUTO mode.	1	24
Scheduling	Monitor scheduling bar in Area 3 and respond to the activated communication with keyboard immediately.	1	24
Resource Management	Monitor oil volume in tanks and pump status in Area 4. Click the corresponding oil pump with a mouse when a failure occurs.	1	24

The NASA-TLX results showed that the overall scores gradually increased with the increase in MW levels (LMW: 39.8 $\pm$ 15.0; HMW: 63.7 $\pm$ 8.2), which means that different task frequencies had successfully caused differences in MW levels. In addition, to find out if MW experiments were not affected by fatigue or emotional factors, subjects were required to fill the Positive and Negative Affect (PANAS) [34] scale and Karolinska Sleepiness Scale (KSS) [35] before and after each MATB task, separately. We calculated the average results of PANAS and KSS scales before and after experiments. The average positive emotion data of PANAS were 25.655 and 25.367, and the average negative emotion data of PANAS were 12.733 and 12.931. The ratios of positive and negative emotion changes were 0.9888 and 1.0156, respectively, which means that subjects were not affected by emotion significantly during the MW experiments. The average results of KSS were 4.333 and 5.931, respectively, which means that the subjects were not overly alert or fatigued before and after experiments.

2.1.2. Data Preprocessing

To reduce the influence of various noises and artifacts in EEG signals on MW classification, it is necessary to remove these artifacts. Firstly, the re-reference of original EEG signals is reset as the average value of M1 and M2. The re-referenced EEG signals are filtered with a 1–30 Hz Finite Impulse Response (FIR) band-pass filter. The temporary artifacts

are manually rejected by using Independent Components Analysis (ICA) according to Reference [36]. It is noted that the EEG data are not normalized after then. According to the 10–20 system, which is endorsed as the standard of the American Electroencephalographic Society (AES) and the International Federation of Societies for Electroencephalography and Clinical Neurophysiology (IFSECN), 26 channels are retained as analyzed channels except for F11, F12, FT11, FT12, M1 and M2. Therefore, 26-channel EEG data without artifact components are obtained. EEG signals for every MW level are preprocessed as above and are used for subsequent analysis and calculations.

2.2. MW Classification Method Based on Selected Sensitive Channels

2.2.1. MW Levels Visualization Method Based on Heatmap

Studies have shown that the PSD at different frequencies can represent the voltage fluctuations under different MW levels [37–39]. The EEG signals can be divided into four rhythms according to the frequency band distribution: δ (1–4 Hz), θ (4–8 Hz), α (8–12 Hz) and β (12–30 Hz). The multitaper spectral estimation method based on PSD is used to calculate the average PSDs in one epoch of each channel [40,41], namely $p_{freq,ch}(i)$. Then energy values are obtained by summing individual $p_{freq,ch}(i)$ in the specific frequency band, as shown in Equation (1).

$$\begin{aligned} E^*_{\delta,ch}(i) &= \sum_{freq=1}^{4} p_{freq,ch}(i) \\ E^*_{\theta,ch}(i) &= \sum_{freq=4}^{8} p_{freq,ch}(i) \\ E^*_{\alpha,ch}(i) &= \sum_{freq=8}^{12} p_{freq,ch}(i) \\ E^*_{\beta,ch}(i) &= \sum_{freq=12}^{30} p_{freq,ch}(i) \end{aligned} \tag{1}$$

where *ch* represents the EEG channel, and there are 26 channels to analyze in this study; *i* represents the epoch, $i = 1, 2, \ldots I$, and I is the number of epochs; $E^*_{\delta,ch}(i)$, $E^*_{\theta,ch}(i)$, $E^*_{\alpha,ch}(i)$ and $E^*_{\beta,ch}(i)$ are the energy values of channel *ch* for δ, θ, α and β in the *i*th epoch, respectively; $p_{freq,ch}(i)$ refers to the average PSDs of the channel *ch* in the *i*th epoch at a certain frequency.

The middle 11-min cleaned EEG data are chosen for further analysis. According to the previous studies [42], the time length of an epoch is set to 2 s, and there are 330 epochs for the 11-min EEG signals in an MW level experiment. Thus $I = 330$ in this study. The frequency sampling interval is 1.42 Hz.

The relative power spectrum is obtained by normalizing the absolute power spectral

$$\begin{gathered} E_{all,ch}(i) = \sum_{freq=1}^{30} p_{freq,ch}(i) \\ E_{\delta,ch}(i) = \frac{E^*_{\delta,ch}(i)}{E_{all,ch}(i)}, E_{\theta,ch}(i) = \frac{E^*_{\theta,ch}(i)}{E_{all,ch}(i)}, E_{\alpha,ch}(i) = \frac{E^*_{\alpha,ch}(i)}{E_{all,ch}(i)}, E_{\beta,ch}(i) = \frac{E^*_{\beta,ch}(i)}{E_{all,ch}(i)} \end{gathered} \tag{2}$$

where $E_{all,ch}(i)$ refers to the PSD at 1–30 Hz; $E_{\delta,ch}(i)$, $E_{\theta,ch}(i)$, $E_{\alpha,ch}(i)$ and $E_{\beta,ch}(i)$ are four relative energy values of the *i*th epoch of channel *ch*, respectively.

EEG energy for every MW level is calculated using Equations (1) and (2). EEG rhythm energy matrixes of Sub *m* in channel *ch* are recorded as $E^L_{m,ch}$ and $E^H_{m,ch}$ with Label *L* and *H* in the upper right-hand corner to represent the levels of LMW and HMW, respectively. It is worth noting that $E^L_{m,ch} = [E^L_{\delta,ch}, E^L_{\theta,ch}, E^L_{\alpha,ch}, E^L_{\beta,ch}]^T$, $E^L_{m,ch} \in \mathbb{R}^{4\times 330}$ and it is similar for $E^H_{m,ch}$.

To reveal the relationship between EEG energy and MW levels in each EEG channel, we refer to the visualization method of cluster analysis in gene sequences [43,44] and first establish an EEG rhythm energy heatmap. $E^L_{m,ch}$ and $E^H_{m,ch}$ of 26 channels are plotted together to observe the change trends of four EEG rhythm energies with epochs or time, EEG channels and MW levels. $E^L_{m,ch}$ is uniformly placed above $E^H_{m,ch}$ for a better comparison.

It should be noted that the Latin square design was used in experiments, so the sequence of LMW and HMW shown in the heatmap is not the real MW test sequence in the experiments. Take $E^L_{\delta,ch}$ and $E^H_{\delta,ch}$ of Sub 5 in the first experiment as an example, Figure 2 shows the visualization process of $E^L_{5,ch}$ and $E^H_{5,ch}$. The $\min(E^L_{\delta,ch}, E^H_{\delta,ch})$ and $\max(E^L_{\delta,ch}, E^H_{\delta,ch})$ are set as the upper and lower limits in the color palette of color mapping, separately. The presented energy–channel–epoch heatmap can reveal the relationship between MW levels, EEG channels and energy values.

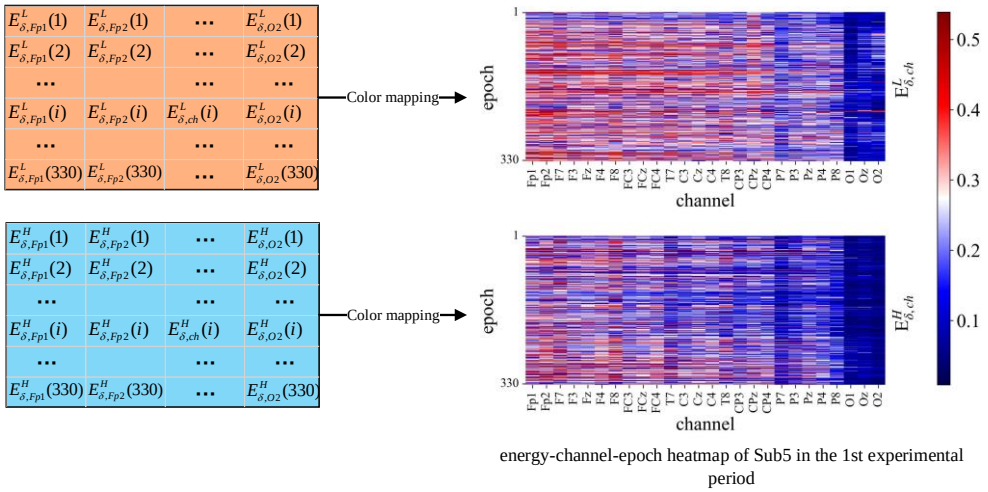

Figure 2. Energy–channel–epoch heatmap drawing flow.

In the energy–channel–epoch heatmap, the y-axis on the left represents epochs in chronological order, the x-axis at the bottom corresponds to 26 EEG channels, and the y-axis color palette on the right visualizes the EEG energy with a color gradient and the color palette. Same rhythm energy values in low and high MW levels, $E^L_{\delta,ch}$ and $E^H_{\delta,ch}$, are plotted together to compare directly. It is similar to the visualization process of the other three EEG rhythm energy. Observational analysis of heatmaps lay the foundation for sensitive selection, and we built a mathematical method to implement this process rather than observation.

2.2.2. Selection Method of Sensitive Channels

A double threshold method is proposed to select the personalized sensitive channels. The double threshold method involves two threshold coefficients: the sensitivity coefficient threshold, *sens*, and the correlation coefficient threshold, *corr*. Here *sens* and *corr* are both in the range between 0 and 1.

In this method, the first step is to judge the sensitivity of 26 channels, and then they will be divided into three types: positive sensitivity channel (PSC), negative sensitivity channel (NSC) and insensitive channel. For the decomposed matrixes, $E^L_{m,ch}$ and $E^H_{m,ch}$, their energy forward differences are used to represent the sensitivity, as shown in Equation (3).

$$\Delta E_{m,ch} = E^H_{m,ch} - E^L_{m,ch} \tag{3}$$

where $\Delta E_{m,ch}$ is energy forward differences of channel ch for Sub m.

If $\Delta E_{m,ch} > 0$, the channel ch is the PSC; if $\Delta E_{m,ch} < 0$, the channel ch is the NSC; if $\Delta E_{m,ch} = 0$, the channel ch is the insensitive channel.

The second step is to calculate the sensitivity coefficient to select sensitive channels using the sensitivity coefficient threshold. For channel ch of Sub m, $\Delta E_{m,ch}$ is calculated in every epoch, and the times of $\Delta E_{m,ch} > 0$ are obtained for all 330 epochs. Let $P_{m,ch}$ and $N_{m,ch}$ be the times that channel ch is deemed to be PSC and NSC, respectively. Define the positive sensitivity index of channel ch as $sen^{po}_{m,ch} = P_{m,ch}/I$ and the negative sensitivity index as $sen^{ne}_{m,ch} = N_{m,ch}/I$. The sensitivity coefficient threshold of channel ch is denoted

as $sens_m$. All channels that meet $sen^{po}_{m,ch} \geq sens_m$ are marked with 1, namely PSCs; all channels that meet $sen^{ne}_{m,ch} \geq sens_m$ are marked with -1, namely NSCs; others are marked with 0. Therefore, 26-tuple vectors of each rhythm, described as $X^*_{m,\delta}$, $X^*_{m,\theta}$, $X^*_{m,\alpha}$ and $X^*_{m,\beta}$, are obtained, which represent the results of sensitive channel selection marked with 0, 1 and -1. The selection results of PSCs and NSCs for the four rhythms can be denoted as $X^*_m = [X^*_{m,\delta}, X^*_{m,\theta}, X^*_{m,\alpha}, X^*_{m,\beta}]^T$, $X^*_m \in \mathbb{R}^{4\times 26}$.

The third step is to calculate the Pearson correlation coefficients for PSCs and NSCs, and select sensitive channels using the correlation coefficient threshold. Energy values of low and high MW levels are simultaneously used to calculate the correlation coefficient between channels. Thus, the energy matrix used for the correlation coefficient calculation can be recorded as $E_{m,ch} = [E^L_{m,ch}, E^H_{m,ch}]$, $E_{m,ch} \in \mathbb{R}^{4\times 660}$. The Pearson coefficient between them can be obtained with Equation (4).

$$corr_m(ch1, ch2) = \frac{\mathrm{cov}(E_{m,ch1}, E_{m,ch2})}{\sigma_{E_{m,ch1}} \sigma_{E_{m,ch2}}} \tag{4}$$

where $corr_m(ch1, ch2)$ represents the Pearson correlation coefficient of four EEG rhythm energies of channels $ch1$ and $ch2$, and $corr_m(ch1, ch2) \in \mathbb{R}^{4\times 2\times 2}$; $ch1$ belongs to PSCs or NSCs of each rhythm selected in the second step, and $ch2$ is any one of 26 channels; $\mathrm{cov}(E_{m,ch1}, E_{m,ch2})$ is the covariance of $E_{m,ch1}$ and $E_{m,ch2}$; $\sigma_{E_{m,ch1}}$ and $\sigma_{E_{m,ch2}}$ represent the standard deviation of $E_{m,ch1}$ and $E_{m,ch2}$, respectively.

The correlation coefficient threshold of Sub m is denoted as $corr_m$. If channel $ch2$ satisfies $corr_m(ch1, ch2) \geq corr_m$, it is marked with 1 when $ch1$ corresponds to PSCs in X^*_m. Similarly, if the channel $ch2$ meets $corr_m(ch1, ch2) \geq corr_m$, it is marked with -1 when $ch1$ corresponds to NSCs in X^*_m. Others are marked with 0. Therefore, a 26-tuple vector is obtained for each $ch1$. Then two 26-tuple vectors are obtained by operating logical conjunction on all 26-tuple vectors when $ch1$ belongs to PSCs and NSCs of each rhythm energy, separately. Finally, new 26-tuple vectors of each rhythm energy, described as $X_{m,\delta}$, $X_{m,\theta}$, $X_{m,\alpha}$ and $X_{m,\beta}$, are obtained by calculating the sum of the two 26-tuple vectors. PSCs' and NSCs' selection results for the four EEG rhythm energy can be denoted as $X_m = [X_{m,\delta}, X_{m,\theta}, X_{m,\alpha}, X_{m,\beta}]$, $X_m \in \mathbb{R}^{4\times 26}$. X_m is used to complete the feature extraction for MW classification in the next subsection.

2.2.3. Feature Extraction Method

This section will mainly describe the feature extraction method based on the selected PSCs and NSCs. Take the MW feature extraction of δ rhythm as an example. According to Equation (2), the δ rhythm energy of 26 channels can be represented as $E_{m,\delta} = [E^L_{m,\delta}, E^H_{m,\delta}]$, where $E^L_{m,\delta} = [E^L_{\delta,Fp1}, E^L_{\delta,Fp2}, \ldots, E^L_{\delta,ch}, \ldots, E^L_{\delta,O2}]^T$, $E^L_{m,\delta} \in \mathbb{R}^{26\times 330}$, and it is similar to $E^H_{m,\delta}$. According to the definition of sensitivity in Equation (3), there is a negative correlation between PSCs and NSCs, so the energy difference in the PSCs and NSCs is calculated to offset the opposite sensitivity. The MW features can be calculated by Equation (5).

$$F_{m,\delta} = X_{m,\delta} \cdot E_{m,\delta} \tag{5}$$

where $F_{m,\delta}$ represents the δ rhythm energy features extracted from Sub m.

The feature extraction calculations for θ, α and β rhythms are the same as the δ rhythm, according to Equation (5). Hence, the energy features of Sub m can be described as $F_m = [F_{m,\delta}, F_{m,\theta}, F_{m,\alpha}, F_{m,\beta}]$. It is worth noting that the feature dimension of Sub m is determined by the rank of the matrix X_m, namely $F_m \in \mathbb{R}^{rank(X_m)\times 660}$. If $rank(X_m) = 0$, it can be regarded that the EEG energy features of the subject are insensitive to these MW experiments and the energy features are not separable.

2.2.4. Classification Algorithm

In this study, the traditional Support Vector Machine (SVM) [45] algorithm is used to classify MW levels even though several SVM augmentations have been developed [46]. The features extracted with Equation (5) are randomly divided into the training set and the validation set by a ratio of 70% to 30%. The grid search method is used to obtain the optimal model parameters on the training set. The search space of the kernel function is {linear, rbf}, the penalty coefficient C is optimized from {0.1, 1, 10, 100} and the kernel parameter γ required for the rbf kernel function is optimized from {0.01, 0.1, 1, 10}. To ensure model robustness and reduce overfitting, the five-fold cross-validation is performed in the classification algorithm.

3. MW Classification Results and Analysis

In this section, the energy–channel–epoch heatmaps and sensitive selection results are analyzed. The proposed sensitive channel selection method and feature extraction method are applied to MW classification. The classification performance of MW is compared with the existing method.

3.1. Analysis of Energy–Channel–Epoch Heatmaps

For the four rhythms of Sub m in every experimental period, four energy–channel–epoch heatmaps have been plotted by the visualized method in Section 2.2.1. The heatmaps can help us to visually and directly observe the sensitivity of channels to tasks. The same rhythm energy values of one subject in the same experimental period are plotted in one subgraph. Three aspects are further analyzed using the heatmap as follows.

1. **The change trend of the four rhythm energies in the heatmaps for the same subject in the same experimental period.**

If we take Sub 1 as an example, Figure 3a–d show the energy–channel–epoch heatmaps of the four rhythms in the first experimental period.

As seen in Figure 3a,b, the δ and θ rhythm energy values of all channels decrease with the increase in MW levels, and the downward trend corresponds to the O1, Oz and O2 channels in the occipital region, which is particularly significant. In Figure 3c, the blue color of the forehead region becomes lighter with the increase in MW levels, which means the α rhythm energy has a slight increase trend, but the energy of the pillow region shows a significant decreasing trend. In Figure 3d, the β rhythm energy of all channels shows an increasing trend as MW levels go from low to high, and the trend of the occipital region is particularly obvious. The change is the opposite to the δ and θ rhythm energy values in Figure 3a,b.

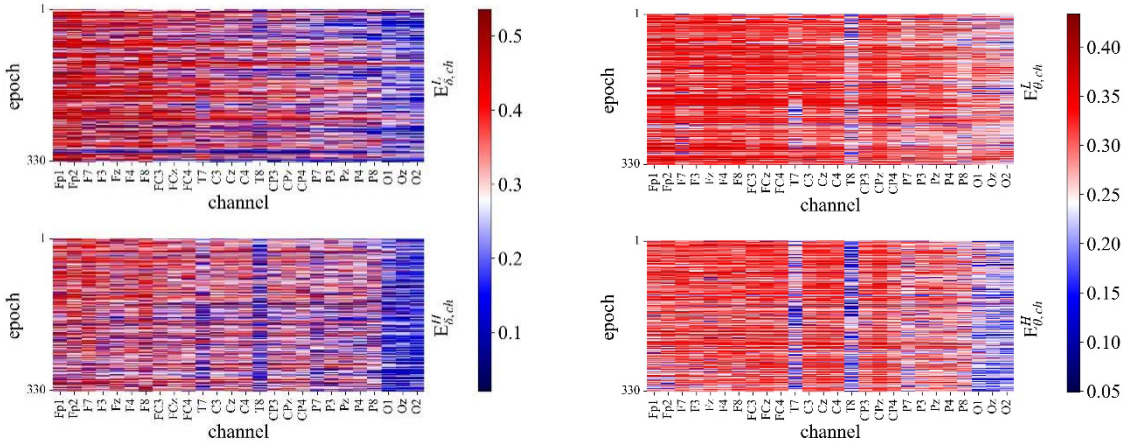

(**a**) δ rhythm (**b**) θ rhythm

Figure 3. *Cont.*

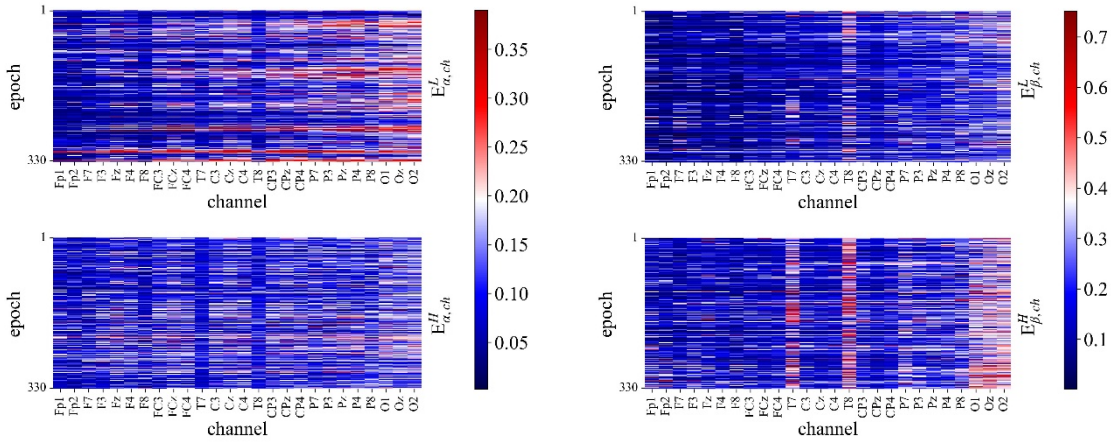

(**c**) α rhythm (**d**) β rhythm

Figure 3. Energy–channel–epoch heatmaps for Sub 1 in the first experimental period.

From the above analysis, it can be concluded that the overall EEG rhythm energy values change with MW levels for the same subject in the same experimental period, but their change trends vary with rhythms and channels.

2. **The change trend of one rhythm energy in the heatmaps for the same subject in different experimental periods.**

If we take Sub 8 as an example, Figure 4a,b show the energy–channel–epoch heatmaps of α rhythm in the first to fourth experimental periods.

As seen from each subgraph, the rhythm energy values in the forehead region increase with the increase in MW levels, but with a downward trend near the occipital region. The overall change trend of the α rhythm energy is similar in the four experiments.

From the above analysis, it can be concluded that the change trend of the overall EEG rhythm energy values with MW levels is the same for the same rhythm of the same subject in different experimental periods, but varies with channels.

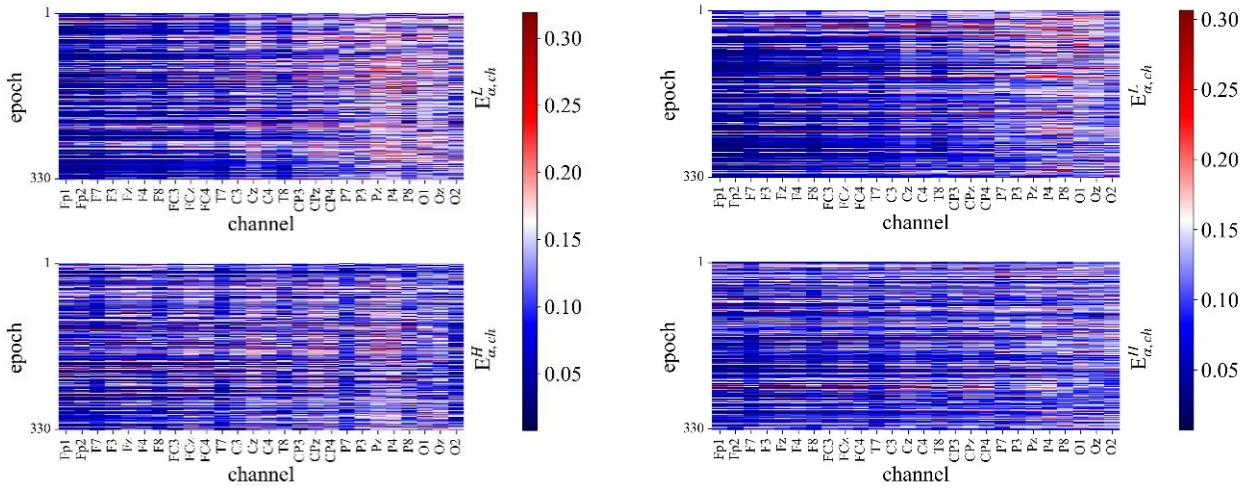

(**a**) On the morning of 1st day (**b**) On the afternoon of 1st day

Figure 4. *Cont.*

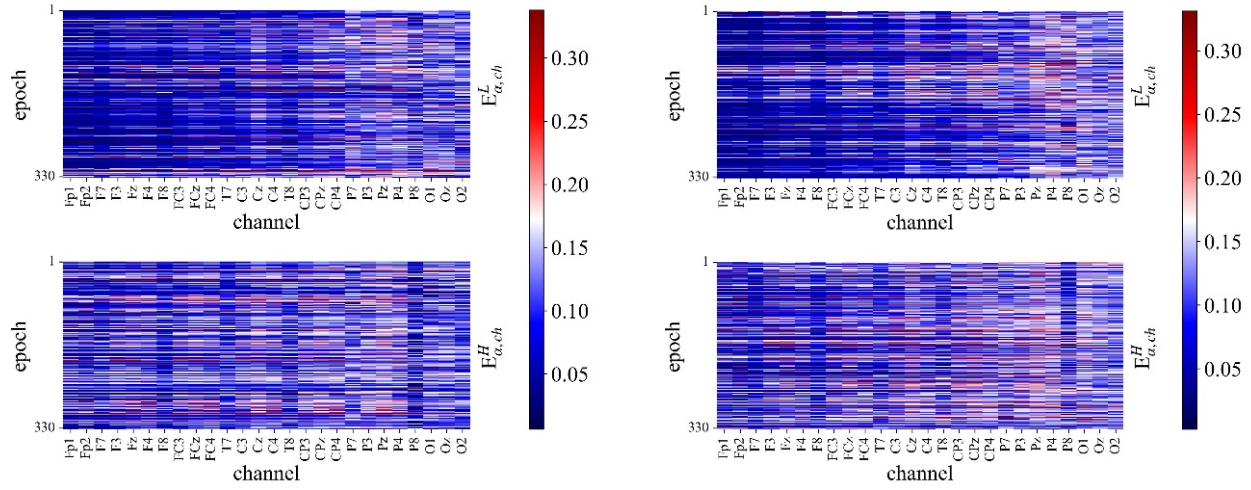

(**c**) On the morning of 2nd day (**d**) On the afternoon of 2nd day

Figure 4. Energy–channel–epoch heatmaps of α rhythm for Sub 8 in 1st to 4th experimental periods.

3. **The change trend of one rhythm energy in the heatmaps for different subjects in the same experimental period.**

If we take the second experimental period as an example, Figure 5a–d show energy–channel–epoch heatmaps of the α rhythm energies of Sub 1, 3, 7 and 9.

As seen from Figure 5a, the α rhythm energies in the forehead region move upwards with the increase in MW levels, but there is a downward trend in the occipital region. In Figure 5b, an upward trend in the overall energies can be observed in all EEG channels as MW levels move from low to high. In Figure 5c, the blue color of the forehead region becomes lighter with the increase in MW levels, which means the α rhythm energy has an increasing trend, but the energy of the central region and pillow region shows a significant decrease trend. In Figure 5d, a downward trend of the overall energies can be observed in all EEG channels with the increase in MW levels.

From the above analysis, it can be concluded that the change trends of the four EEG rhythm energies with different MW levels vary with subjects and channels even in the same experimental period.

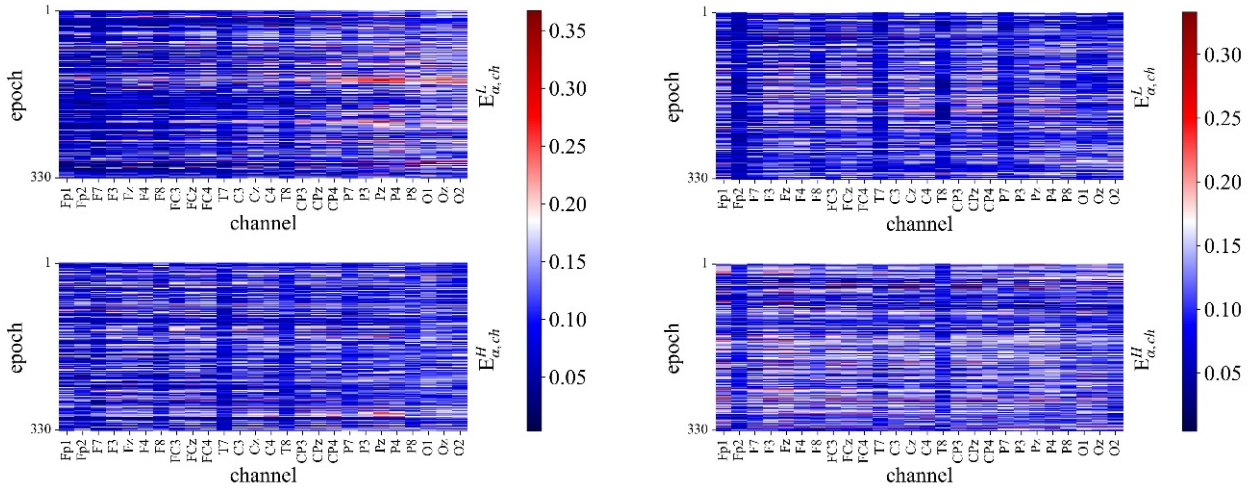

(**a**) Sub 1 (**b**) Sub 3

Figure 5. *Cont.*

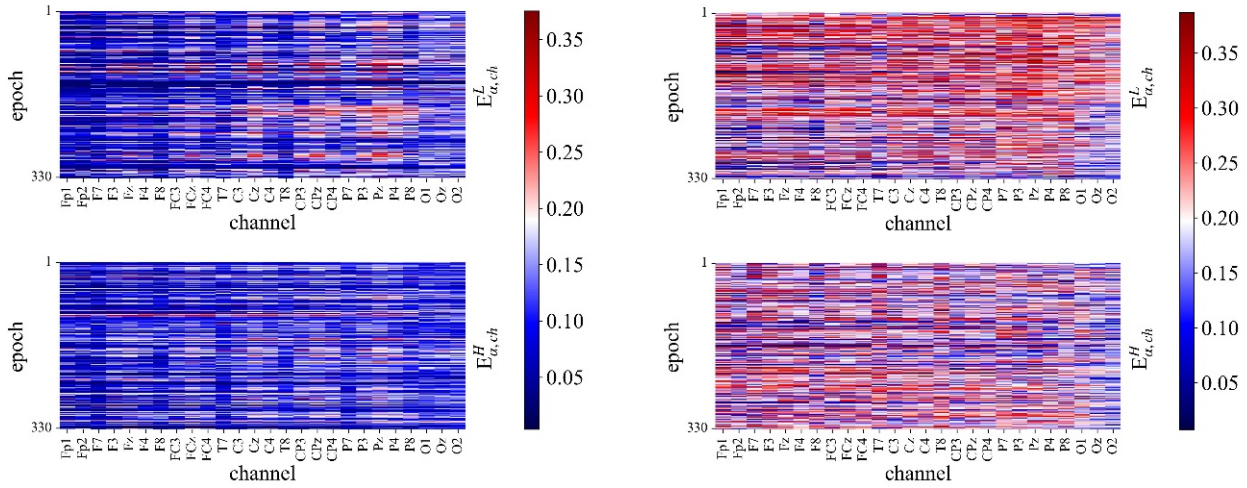

(**c**) Sub 7 (**d**) Sub 9

Figure 5. Energy–channel–epoch heatmaps of α rhythm for Subs 1, 3, 7 and 9 in the 2nd experimental period.

Based on the above analysis of the energy–channel–epoch heatmaps, some conclusions can be obtained:

(1) The energy value in one epoch cannot represent the MW level very well.
(2) For the same subject, the four EEG rhythm energy values change with the MW level steadily. This means that the sensitivity of channel energy to MW levels is also stable with time in the short term. It should be noted that this conclusion is based on the experimental conditions and other objective factors being the same.
(3) The sensitivity of the EEG channels to MW levels is divided into three types: positive sensitivity (energy value is positively correlated with MW levels), negative sensitivity (energy value is negatively correlated with MW levels) and insensitivity.
(4) $E_{\delta,ch}$, $E_{\theta,ch}$, $E_{\alpha,ch}$ and $E_{\beta,ch}$ separately and regularly vary with MW levels, but their degrees of change are different among subjects.

3.2. Analysis of Sensitivity Threshold

The MW classification method with the features extracted with Equation (5) involves two threshold variables: $sens_m$ and $corr_m$. The correlation coefficient threshold is set as $corr_m = 0.95$ for all subjects. The influence of different $sens_m$ on MW classification is analyzed as follows.

The search space of $sens_m$ is set as {0.55, 0.6, 0.65, 0.7, 0.75, 0.8, 0.85, 0.9}. The features extracted from the EEG data for two experiments on the first day are used as the training data for MW classifier construction. The features extracted from the EEG data for the two experiments on the second day are used as test data, and the feature extraction of the test set is based on the sensitive channel selection results of the training set. Test accuracies with different sensitivity coefficient thresholds are shown as follows:

From Figure 6, some conclusions can be drawn:

(1) The MW classification accuracies of Subs 3, 5 and 8 are positively correlated with sens.
(2) The values of sens for Subs 1, 2, 4, 6 and 10 are non-monotonic.
(3) The relationship between classification accuracy and sens is roughly negative for Subs 1 and 9.

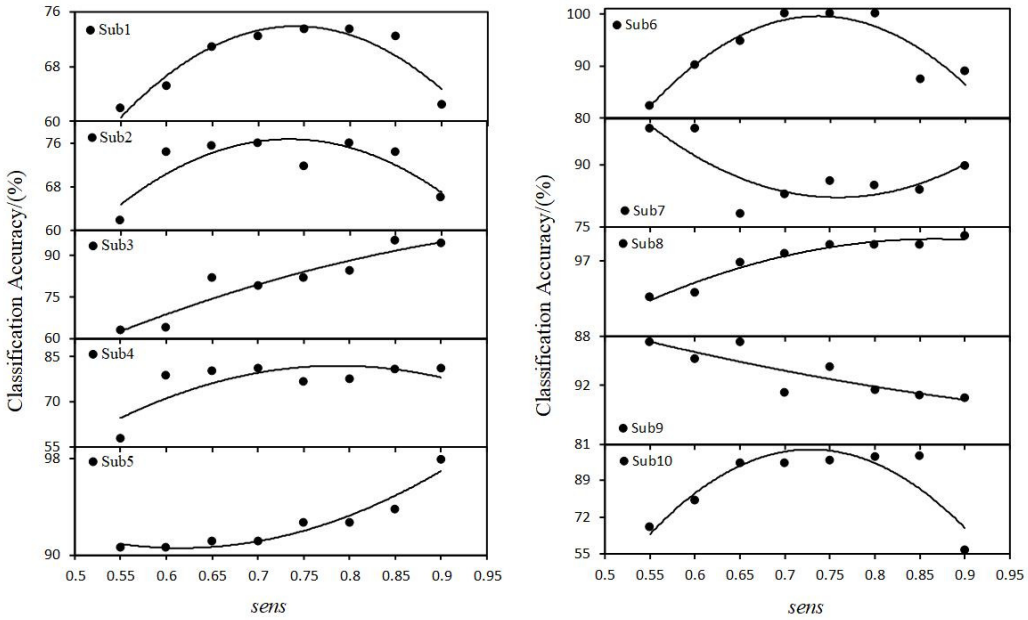

Figure 6. Comparison of MW classification accuracy corresponds to different sensitivity coefficient thresholds.

According to the polynomial curve fitting in Figure 6, the optimal and worst *sens* of each subject can be obtained, as shown in Table 2.

Table 2. Classification results with optimal and worst *sens*.

Subject	Optimal		Worst	
	$sens_m$	Test Accuracy (%)	$sens_m$	Test Accuracy (%)
Sub 1	0.75	73.44	0.55	61.98
Sub 2	0.7	76.04	0.55	61.98
Sub 3	0.9	94.27	0.55	63.02
Sub 4	0.7	81.25	0.55	57.81
Sub 5	0.9	97.92	0.55	90.63
Sub 6	0.75	100	0.55	82.29
Sub 7	0.55	98.44	0.9	89.58
Sub 8	0.9	100	0.55	92.71
Sub 9	0.55	100	0.9	89.58
Sub 10	0.8	99.48	0.9	56.77

From Table 2, we can observe that:

(1) The accuracy with the optimal *sens* ranges from 73.44% to 100%, and the average is 92.08%.
(2) The accuracy with the worst *sens* ranges from 56.7% to 92.71%, and the average is 74.64%.
(3) The improvement in test accuracy for each subject ranges from 7.29% to 42.71%, and the average is 17.45%.

3.3. Selection Results with Optimal MW Classification Accuracy

If we take Subs 1 and 8 as examples, this section shows the channel selection results with the optimal *sens* in Table 2, namely $sens_1 = 0.75$ and $sens_8 = 0.9$. EEG channel diagrams of the four rhythms are shown in Figures 7 and 8. The channels are marked with a red or blue color, which means that the energies presented in the four rhythms of certain channels are sensitive to MW levels. The red and blue color channels represent the PSCs and NSCs, respectively. Their corresponding values are 1 and -1 in matrix X_m, respectively.

The black color channels represent insensitive channels and their values are 0 in matrix X_m. For Subs 1 and 8, their feature dimensions are both four, namely $rank(X_1) = 4$ and $rank(X_8) = 4$, respectively.

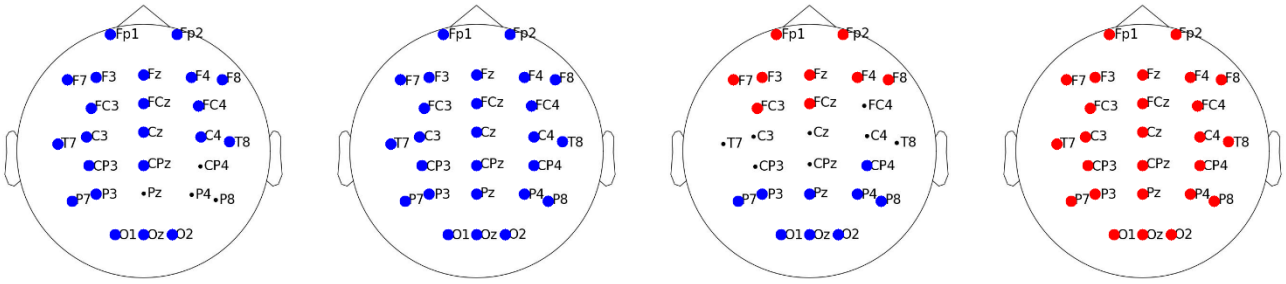

(**a**) δ rhythm (**b**) θ rhythm (**c**) α rhythm (**d**) β rhythm

Figure 7. PSCs and NSCs for four rhythms of Sub 1.

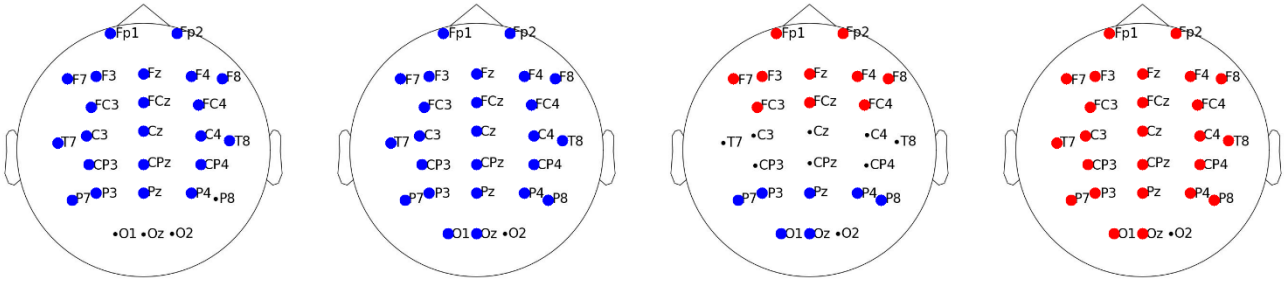

(**a**) δ rhythm (**b**) θ rhythm (**c**) α rhythm (**d**) β rhythm

Figure 8. PSCs and NSCs for four rhythms of Sub 8.

For Sub 1, Figures 3 and 7 reflect different aspects of the four EEG rhythm energies. Figure 7 shows the sensitive channel selection results of the PSCs and the NSCs, and Figure 3 shows the energy–channel–epoch heatmaps. Figures 4 and 8c show similar results for Sub 8. From Figures 3, 4, 7 and 8, the results of the sensitive channel selection are consistent with the heatmaps.

Comparing the sensitive channel selection diagrams with the energy–channel–epoch heatmaps, some conclusions can be observed:

(1) In Figure 7a, almost all channels are marked as NSCs for the δ and θ rhythm energies. It means that the δ and θ rhythm energies decrease with the increase in MW levels, which corresponds to the trend shown in Figure 3a,b.

(2) In Figure 7c, the red channels in the forehead region and the blue channels in the occipital region are consistent with the increase in alpha rhythm energies in the forehead region and the decrease in the occipital region shown in Figure 3c, respectively.

(3) In Figure 7d, 26 channels are selected as PSCs, which means that the beta rhythm energies of all channels increase with MW levels, which is consistent with the information shown in Figure 3d.

(4) In Figure 8c, the channels in the forehead are marked as PSCs with a red color and the channels in the occipital regions are marked as NSCs with a blue color, which is the same as the analysis results of Figure 4.

3.4. Comparison of MW Classification Using Sensitive Channels and All Channels

Two MW classification methods are compared in this section. The former method presented in this study is named Method 1 using the selected sensitive channels, and the latter is named Method 2 using all channels.

Method 1: It is proposed in this study to build MW classifiers based on the PSCs and the NSCs. In this method, after calculating the four EEG rhythm energies, the PSCs and the NSCs of the four rhythms are selected by the double threshold method, and then the selection results are used to obtain the MW features with Equation (4). The feature dimension is determined by the sensitive channel selection results. Finally, these features are used for training using the SVM.

Method 2: This realizes an MW classification by using all rhythm energies from 26 channels. This method directly extracts MW features by calculating the sum of the rhythm energies of 26 channels. The features calculated by Method 2 are 4-dimensional for each subject. Then the features are used for training using the SVM with the same parameter settings as in Section 2.2.4.

To observe the influence of sensitive selection on MW classification, test accuracies with the optimal and worst values of *sens* in Method 1, as shown in Table 2, are compared with the test accuracies of Method 2, as shown in Figure 9. The max and min values of the classification accuracies of Method 1 are obtained by setting the optimal and worst *sens*, respectively.

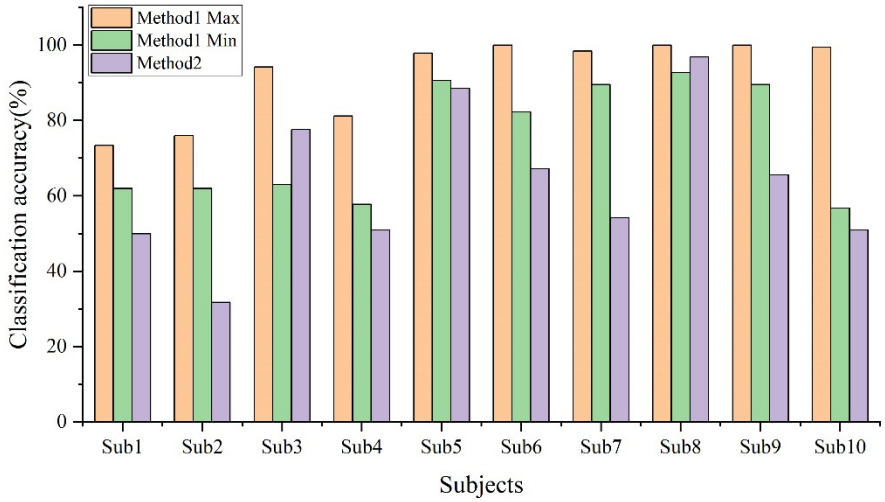

Figure 9. Classification accuracy comparison of Method 1 and Method 2.

From Figure 9, some conclusions can be observed:

(1) The accuracies of Method 2 range between 31.77% and 96.88%, and the average accuracy is 63.39%.
(2) The accuracies of Method 1 with the optimal *sens* are higher than those of Method 2, and the improvement in the test accuracy ranges between 3.13% and 48.44% with an average of 28.69%.
(3) The accuracies of Method 1 with the worst *sens* are mostly higher than those of Method 2 except for Subs 3 and 8, and the improvement in the test accuracy ranges between 2.08% and 35.42% with an average of 11.25%.

4. Discussion

It is possible to explore the regularity of rhythmic energy in various channels with different MW levels. In the current literature, the channel selection problem is often regarded as a complex multi-objective optimization problem. However, in this study, the energy visualization method is presented for the first time to show the multi-information of EEG signals simultaneously, including time, frequency and spatial domain information. The energy–channel–epoch heatmaps generated by this method reveal that the overall EEG energies of each channel sensitively vary with MW levels, but this change varies for different rhythms and subjects. There are three tendencies for EEG rhythm energies changing with the increase in MW levels: positive sensitive, negative sensitive and insensitive. However,

the trend varies with subjects, rhythms and channels. The energy of a single epoch cannot interpret the MW level effectively; that is, the energy features extracted from EEG signals that are too short might be unfavorable to classification accuracy. In future work, we will further investigate the stability of the optimal signal length for MW classification and the temporal stability of EEG energy changing with MW levels.

This study provides a new idea for similar research in other fields of machine learning with multi-information relevance. However, the presented double threshold method for sensitive EEG channel selection has a limit for obtaining the optimal sensitivity coefficient threshold for each subject, therefore, a pre-experiment should be carried out in order to ensure good MW classification accuracy.

5. Conclusions

The brain activation region stimulated by MW tasks is not the same for every subject. In this paper, heatmaps are presented to visualize the change trends of four EEG rhythm energies with time, EEG channels and MW levels. Then a double threshold method is proposed to select sensitive channels according to the analysis results of the heatmaps. The selection results are consistent with the analysis of energy–channel–epoch heatmaps. The PSCs, NSCs and insensitive channels are specially labeled as 1, −1 and 0. Their features are extracted and are used to train an MW classifier with the SVM algorithm.

Some conclusions can be obtained:

(1) Selection results of sensitive channels

The personalized sensitivity threshold of each subject obtained by experiments finally determines the selection results of sensitive channels. A too high or too low sensitivity threshold may reject some channels containing useful information or introduce redundant channel information.

(2) Classification accuracy comparisons

The results show that the MW classification accuracy of the presented method using selected channels is between 73.43% and 100% with an average accuracy of 92.08%. Compared with the method using all EEG channels, the classification accuracies with the worst *sens* are still higher for most subjects and the average accuracy is improved by 11.25%. With the optimal *sens*, the test accuracy can be improved from 3.13% to 48.44%, and the average accuracy can be improved by 28.69%. The results show that sensitive channels can contribute to the improvement in MW classification accuracy.

Author Contributions: Conceptualization, H.Q.; methodology, H.Q.; software, L.J.; validation, H.Q., L.J. and Z.Z.; formal analysis, H.Q.; investigation, L.J.; resources, L.P.; data curation, L.J.; writing—original draft preparation, L.J.; writing—review and editing, L.J. and L.P.; visualization, L.J.; supervision, H.Q. and Z.Z.; project administration, H.Q.; funding acquisition, L.P. All authors have read and agreed to the published version of the manuscript.

Funding: This research received no external funding.

Institutional Review Board Statement: The study was conducted in accordance with the Declaration of Helsinki, and approved by the Institutional Biological and Medical Ethics Committee, Beihang University (protocol code BM201900078, June 2019).

Informed Consent Statement: Informed consent was obtained from all subjects involved in the study.

Data Availability Statement: The data presented in this study are available on request from the corresponding author. The data are not publicly available due to confidentiality issues.

Acknowledgments: The authors are grateful to the subjects for their contributions to the experiment.

Conflicts of Interest: The authors declare no conflict of interest.

References

1. Pereira da Silva, M. Mental Workload, Task Demand and Driving Performance: What Relation? *Procedia Soc. Behav. Sci.* **2014**, *162*, 310–319. [CrossRef]
2. Wilson, G.F. Operator Functional State Assessment for Adaptive Automation Implementation. In Proceedings of the Biomonitoring for Physiological and Cognitive Performance during Military Operations, Orlando, FL, USA, 31 March–1 April 2005; SPIE: Bellingham, WA, USA, 2005; Volume 5797, pp. 100–104.
3. Lu, Y.; Bi, L. EEG Signals-Based Longitudinal Control System for a Brain-Controlled Vehicle. *IEEE Trans. Neural Syst. Rehabil. Eng.* **2019**, *27*, 323–332. [CrossRef]
4. Hekmatmanesh, A.; Zhidchenko, V.; Kauranen, K.; Siitonen, K.; Handroos, H.; Soutukorva, S.; Kilpelainen, A. Biosignals in Human Factors Research for Heavy Equipment Operators: A Review of Available Methods and Their Feasibility in Laboratory and Ambulatory Studies. *IEEE Access* **2021**, *9*, 97466–97482. [CrossRef]
5. Sikander, G.; Anwar, S. Driver Fatigue Detection Systems: A Review. *IEEE Trans. Intell. Transp. Syst.* **2019**, *20*, 2339–2352. [CrossRef]
6. Radüntz, T. Dual Frequency Head Maps: A New Method for Indexing Mental Workload Continuously during Execution of Cognitive Tasks. *Front. Physiol.* **2017**, *8*, 1019. [CrossRef]
7. Hart, S. Nasa-Task Load Index (Nasa-TLX); 20 Years Later. In Proceedings of the Human Factors and Ergonomics Society Annual Meeting, San Francisco, CA, USA, 16–20 October 2006; Volume 50, pp. 904–908.
8. Ryu, K.; Myung, R. Evaluation of Mental Workload with a Combined Measure Based on Physiological Indices during a Dual Task of Tracking and Mental Arithmetic. *Int. J. Ind. Ergon.* **2005**, *35*, 991–1009. [CrossRef]
9. Lemm, S.; Blankertz, B.; Dickhaus, T.; Müller, K.-R. Introduction to Machine Learning for Brain Imaging. *NeuroImage* **2011**, *56*, 387–399. [CrossRef]
10. Schalk, G.; McFarland, D.J.; Hinterberger, T.; Birbaumer, N.; Wolpaw, J.R. BCI2000: A General-Purpose Brain-Computer Interface (BCI) System. *IEEE Trans. Biomed. Eng.* **2004**, *51*, 1034–1043. [CrossRef]
11. Naseer, N.; Hong, K.-S. Classification of Functional Near-Infrared Spectroscopy Signals Corresponding to the Right- and Left-Wrist Motor Imagery for Development of a Brain–Computer Interface. *Neurosci. Lett.* **2013**, *553*, 84–89. [CrossRef]
12. Naseer, N.; Hong, K.-S. FNIRS-Based Brain-Computer Interfaces: A Review. *Front. Hum. Neurosci.* **2015**, *9*, 3. [CrossRef]
13. Aghajani, H.; Omurtag, A. Assessment of Mental Workload by EEG+FNIRS. In Proceedings of the 2016 38th Annual International Conference of the IEEE Engineering in Medicine and Biology Society (EMBC), Orlando, FL, USA, 16–20 August 2016; pp. 3773–3776.
14. Qu, H.; Shan, Y.; Liu, Y.; Pang, L.; Fan, Z.; Zhang, J.; Wanyan, X. Mental Workload Classification Method Based on EEG Independent Component Features. *Appl. Sci.* **2020**, *10*, 3036. [CrossRef]
15. Salimi, N.; Barlow, M.; Lakshika, E. Mental Workload Classification Using Short Duration EEG Data: An Ensemble Approach Based on Individual Channels. In Proceedings of the 2019 IEEE Symposium Series on Computational Intelligence (IEEE SSCI 2019), Xiamen, China, 6–9 December 2019; IEEE: New York, NY, USA, 2019; pp. 393–398.
16. Liu, Y.; Ayaz, H.; Shewokis, P.A. Mental Workload Classification with Concurrent Electroencephalography and Functional Near-Infrared Spectroscopy. *Brain-Comput. Interfaces* **2017**, *4*, 175–185. [CrossRef]
17. Zhang, P.; Wang, X.; Chen, J.; You, W.; Zhang, W. Spectral and Temporal Feature Learning With Two-Stream Neural Networks for Mental Workload Assessment. *IEEE Trans. Neural Syst. Rehabil. Eng.* **2019**, *27*, 1149–1159. [CrossRef] [PubMed]
18. Li, X.; Chen, F.; Jia, Y.; Liu, X. Signal Detection, Processing and Challenges of Non-Invasive Brain-Computer Interface Technology. In Proceedings of the 2019 Chinese Intelligent Automation Conference, Zhanjiang, China, 20–22 September 2019; Deng, Z., Ed.; Springer: Singapore, 2020; pp. 60–67.
19. Sanei, S.; Chambers, J.A. Introduction to EEG. In *EEG Signal Processing*; John Wiley & Sons, Ltd.: Hoboken, NJ, USA, 2007; pp. 15–17. ISBN 978-0-470-51192-3.
20. Acharya, J.N.; Hani, A.; Cheek, J.; Thirumala, P.; Tsuchida, T.N. American Clinical Neurophysiology Society Guideline 2: Guidelines for Standard Electrode Position Nomenclature. *J. Clin. Neurophysiol.* **2016**, *33*, 308–311. [CrossRef] [PubMed]
21. Chen, J.; Taylor, J.E.; Comu, S. Assessing Task Mental Workload in Construction Projects: A Novel Electroencephalography Approach. *J. Constr. Eng. Manag.* **2017**, *143*, 04017053. [CrossRef]
22. Murata, A. An Attempt to Evaluate Mental Workload Using Wavelet Transform of EEG. *Hum. Factors* **2005**, *47*, 498–508. [CrossRef]
23. Wang, X.; Li, D.; Menassa, C.; Kamat, V. Investigating the Effect of Indoor Thermal Environment on Occupants' Mental Workload and Task Performance Using Electroencephalogram. *Build. Environ.* **2019**, *158*, 120–132. [CrossRef]
24. Bagheri, M.; Power, S.D. Simultaneous Classification of Both Mental Workload and Stress Level Suitable for an Online Passive Brain-Computer Interface. *Sensors* **2022**, *22*, 535. [CrossRef]
25. Alotaiby, T.; Abd El-Samie, F.E.; Alshebeili, S.A.; Ahmad, I. A Review of Channel Selection Algorithms for EEG Signal Processing. *EURASIP J. Adv. Signal Process.* **2015**, *2015*, 66. [CrossRef]
26. Alyasseri, Z.A.A.; Khader, A.T.; Al-Betar, M.A.; Alomari, O.A. Person Identification Using EEG Channel Selection with Hybrid Flower Pollination Algorithm. *Pattern Recognit.* **2020**, *105*, 107393. [CrossRef]
27. Li, Y.; Yang, H.; Li, J.; Chen, D.; Du, M. EEG-Based Intention Recognition with Deep Recurrent-Convolution Neural Network: Performance and Channel Selection by Grad-CAM. *Neurocomputing* **2020**, *415*, 225–233. [CrossRef]

28. Moctezuma, L.A.; Molinas, M. Multi-Objective Optimization for EEG Channel Selection and Accurate Intruder Detection in an EEG-Based Subject Identification System. *Sci. Rep.* **2020**, *10*, 5850. [CrossRef] [PubMed]
29. Park, S.-M.; Kim, J.-Y.; Sim, K.-B. EEG Electrode Selection Method Based on BPSO with Channel Impact Factor for Acquisition of Significant Brain Signal. *Optik* **2018**, *155*, 89–96. [CrossRef]
30. Zhu, G.; Zong, F.; Zhang, H.; Wei, B.; Liu, F. Cognitive Load During Multitasking Can Be Accurately Assessed Based on Single Channel Electroencephalography Using Graph Methods. *IEEE Access* **2021**, *9*, 33102–33109. [CrossRef]
31. Altahat, S.; Chetty, G.; Tran, D.; Ma, W. Analysing the Robust EEG Channel Set for Person Authentication. In Proceedings of the International Conference on Neural Information Processing, Istanbul, Turkey, 9–12 November 2015; Arik, S., Huang, T., Lai, W., Liu, Q., Eds.; Springer: Istanbul, Turkey, 2015; Volume 9492, pp. 162–173.
32. Comstock, J.R.; Arnegard, R.J. *The Multi-Attribute Task Battery for Human Operator Workload and Strategic Behavior Research*; NASA Technical Memorandum; National Aeronautics and Space Administration, Langley Research Center: Hampton, VA, USA; National Technical Information Service, Distributor: Springfield, VA, USA, 1992.
33. Feng, C.; Wanyan, X.; Liu, S.; Chen, H.; Zhuang, D.; Wang, X. Influence of different attention allocation strategies under workloads on situation awareness. *Acta Aeronaut. Astronaut. Sin.* **2020**, *41*, 123307. [CrossRef]
34. Watson, D.; Clark, L.A.; Tellegen, A. Development and Validation of Brief Measures of Positive and Negative Affect: The PANAS Scales. *J. Personal. Soc. Psychol.* **1988**, *54*, 1063–1070. [CrossRef]
35. Kaida, K.; Takahashi, M.; Akerstedt, T.; Nakata, A.; Otsuka, Y.; Haratani, T.; Fukasawa, K. Validation of the Karolinska Sleepiness Scale against Performance and EEG Variables. *Clin. Neurophysiol.* **2006**, *117*, 1574–1581. [CrossRef]
36. Jung, T.-P.; Makeig, S.; Humphries, C.; Lee, T.-W.; McKeown, M.J.; Iragui, V.; Sejnowski, T.J. Removing Electroencephalographic Artifacts by Blind Source Separation. *Psychophysiology* **2000**, *37*, 163–178. [CrossRef]
37. Menon, V.; Rivera, S.M.; White, C.D.; Glover, G.H.; Reiss, A.L. Dissociating Prefrontal and Parietal Cortex Activation during Arithmetic Processing. *NeuroImage* **2000**, *12*, 357–365. [CrossRef]
38. Akin, M.; Kurt, M.B.; Sezgin, N.; Bayram, M. Estimating Vigilance Level by Using EEG and EMG Signals. *Neural Comput. Appl.* **2008**, *17*, 227–236. [CrossRef]
39. Chuang, S.-W.; Ko, L.-W.; Lin, Y.-P.; Huang, R.-S.; Jung, T.-P.; Lin, C.-T. Co-Modulatory Spectral Changes in Independent Brain Processes Are Correlated with Task Performance. *NeuroImage* **2012**, *62*, 1469–1477. [CrossRef]
40. Percival, D.B.; Walden, A.T. Spectral Analysis for Physical Applications: Multitaper and Conventional Univariate Techniques. *Technometrics* **1996**, *38*, 294. [CrossRef]
41. Babadi, B.; Brown, E.N. A Review of Multitaper Spectral Analysis. *IEEE Trans. Biomed. Eng.* **2014**, *61*, 1555–1564. [CrossRef] [PubMed]
42. Levy, W.J. Effect of Epoch Length on Power Spectrum Analysis of the EEG. *Anesthesiology* **1987**, *66*, 489–495. [CrossRef] [PubMed]
43. Metsalu, T.; Vilo, J. ClustVis: A Web Tool for Visualizing Clustering of Multivariate Data Using Principal Component Analysis and Heatmap. *Nucleic Acids Res.* **2015**, *43*, 566–570. [CrossRef]
44. Gu, Z.; Eils, R.; Schlesner, M. Complex Heatmaps Reveal Patterns and Correlations in Multidimensional Genomic Data. *Bioinformatics* **2016**, *32*, 2847–2849. [CrossRef]
45. Shao, Y.; Lunetta, R.S. Comparison of Support Vector Machine, Neural Network, and CART Algorithms for the Land-Cover Classification Using Limited Training Data Points. *ISPRS J. Photogramm. Remote Sens.* **2012**, *70*, 78–87. [CrossRef]
46. Tian, Y.; Shi, Y.; Liu, X. Recent Advances on Support Vector Machines Research. *Technol. Econ. Dev. Econ.* **2012**, *18*, 5–33. [CrossRef]